J|A|C|S ARTICLES

Published on Web 04/02/2010

Molecular Basis of Coupled Protein and Electron Transfer Dynamics of Cytochrome *c* in Biomimetic Complexes

Damián Alvarez-Paggi,[†] Diego F. Martín,[†] Pablo M. DeBiase,[†] Peter Hildebrandt,[‡] Marcelo A. Martí,*[,†] and Daniel H. Murgida*[,†]

Departamento de Química Inorgánica, Analítica y Química Física/INQUIMAE-CONICET, Facultad de Ciencias Exactas y Naturales, Universidad de Buenos Aires, Ciudad Universitaria, Pab. 2, piso 1, C1428EHA-Buenos Aires, Argentina, and Technische Universität Berlin, Institut für Chemie, Strasse des 17. Juni 135, Sekr. PC14, D-10623-Berlin, Germany

Received December 19, 2009; E-mail: marcelo@qi.fcen.uba.ar; dhmurgida@qi.fcen.uba.ar

Abstract: Direct electron transfer (ET) of redox proteins immobilized on biomimetic or biocompatible electrodes represents an active field of fundamental and applied research. In this context, several groups have reported for a variety of proteins unexpected distance dependencies of the ET rate, whose origin remains largely speculative and controversial, but appears to be a quite general phenomenon. Here we have employed molecular dynamics (MD) simulations and electron pathway analyses to study the ET properties of cytochrome *c* (Cyt) electrostatically immobilized on Au coated by carboxyl-terminated alkylthiols. The MD simulations and concomitant binding energy calculations allow identification of preferred binding configurations of the oxidized and reduced Cyt which are established via different lysine residues and, thus, correspond to different orientations and dipole moments. Calculations of the electronic coupling matrices for the various Cyt/self-assembled monolayer (SAM) complexes indicate that the thermodynamically preferred protein orientations do not coincide with the orientations of optimum coupling. These findings demonstrate that the ET of the immobilized Cyt is controlled by an interplay between protein dynamics and tunneling probabilities. Protein dynamics exerts two level of tuning on the electronic coupling via reorientation (coarse) and low amplitude thermal fluctuations (fine). Upon operating the Au support as an electrode, electric-field-dependent alignment of the protein dipole moment becomes an additional determinant for the protein dynamics and thus for the overall ET rate. The present results provide a consistent molecular description of previous (spectro)electrochemical data and allow conclusions concerning the coupling of protein dynamics and ET of Cyt in physiological complexes.

Introduction

Electron transfer (ET) reactions of proteins play a central role in a variety of physiological processes as well as in emerging fields of biotechnology such as the development of enzyme-based biosensors and biofuel cells.[1,2] A widely employed approach to analyze these fundamental processes is based on model systems in which redox proteins are immobilized on conducting support materials that provide a biocompatible environment and mimic to some extent the natural reaction conditions.[3−5] Particularly versatile model systems are metal electrodes coated with self-assembled monolayers (SAMs) of ω-functionalized alkanethiols which, upon appropriate choice of the tail group, may bind various proteins via electrostatic, polar, or hydrophobic interactions, or via covalent cross-linking and coordinative bonds.[4−8] Heterogeneous ET between the immobilized protein and the metal electrode involves through-SAM tunneling, and the ET rate constant (k_{ET}) may be described in terms of the high temperature limit of Marcus semiclassical expression (nonadiabatic mechanism), integrated over all the electronic levels of the metal electrode contributing to the process.[9,10] In this formalism, k_{ET} varies with the square of the electronic coupling matrix (T_{DA}), which in turn decays exponentially with the distance between the redox center and the electrode surface. Therefore, for a protein attached to a SAM-coated electrode, k_{ET} is expected to decay exponentially upon increasing the number of methylene groups of the SAMs. This behavior has been experimentally verified for a number of SAM/protein complexes that include cytochromes *c*, c_6 and b_{562}, Cu_A centers and azurin.[11−22] The predicted exponential distance-dependence of the experimentally determined ET rate

[†] Universidad de Buenos Aires.
[‡] Technische Universität Berlin, Institut für Chemie.

(1) Cracknell, J. A.; Vincent, K. A.; Armstrong, F. A. *Chem. Rev.* **2008**, *108*, 2439.
(2) Willner, I.; Katz, E. *Angew. Chem., Int. Ed.* **2000**, *39*, 1180.
(3) Armstrong, F. A. *Curr. Opin. Chem. Biol.* **2005**, *9*, 110.
(4) Murgida, D. H.; Hildebrandt, P. *Acc. Chem. Res.* **2004**, *37*, 854.
(5) Murgida, D. H.; Hildebrandt, P. *Chem. Soc. Rev.* **2008**, *37*, 937.
(6) Fedurco, M. *Coord. Chem. Rev.* **2000**, *209*, 263.
(7) Murgida, D. H.; Hildebrandt, P.; Wei, J.; He, Y. F.; Liu, H. Y.; Waldeck, D. H. *J. Phys. Chem. B* **2004**, *108*, 2261.
(8) Rivas, L.; Murgida, D. H.; Hildebrandt, P. *J Phys. Chem. B* **2002**, *106*, 4823.
(9) Kuznetsov, A. M.; Ulstrup, J. *Electron Transfer in Chemistry and Biology. An Introduction to the Theory*; 1 ed.; Wiley: Chichester, 1999.
(10) Marcus, R. A. *J. Chem. Phys.* **1965**, *43*, 679.
(11) Avila, A.; Gregory, B. W.; Niki, K.; Cotton, T. M. *J. Phys. Chem. B* **2000**, *104*, 2759.
(12) Chi, Q. J.; Zhang, J. D.; Andersen, J. E. T.; Ulstrup, J. *J. Phys. Chem. B* **2001**, *105*, 4669.
(13) Davis, K. L.; Waldeck, D. H. *J. Phys. Chem. B* **2008**, *112*, 12498.

constant (k_{ET}^{app}), however, is only fulfilled for thicker SAMs, i.e. those containing more than nine methylene groups per alkyl chain. For thinner films, in contrast, k_{ET}^{app} appears to be distance independent in all cases investigated so far.[11−22] The origin for this unexpected kinetic behavior has been the subject of intense research as it represents a fundamental issue in bioelectrochemistry, with potential implications for physiological protein ET as well as for technological applications of redox enzymes.

The most extensive studies refer to cytochrome *c* (Cyt) electrostatically or coordinatively bound to SAM-coated electrodes. Different hypothesis have been proposed for explaining the rate-limiting process in the distance-independent regime, including (i) a two-state gating mechanism,[11,18] (ii) an electric-field (EF)-dependent hydrogen-bonding rearrangement,[17,23] and (iii) a change from tunnelling to polarization relaxation control of the ET rate.[19,21]

Recently, we have shown that for electrostatic Cyt/SAM complexes in the plateau region k_{ET}^{app} coincides with the rate of protein reorientation (k_R), as determined by time-resolved surface enhanced resonance Raman (TR-SERR) spectroelectrochemistry.[24,25] The experimental k_R values increase with the chain length of the SAMs, i.e. upon decreasing the strength of the interfacial electric field. On the basis of these results it was proposed that at long distances the kinetics of the reaction is solely controlled by the electron tunnelling probability. At shorter distances, however, reorientation of the immobilized protein to a configuration most favorable for ET becomes rate determining. These results represented the first direct observation of protein dynamics at an electrochemical interface under reactive conditions.[24,25] However, although TR-SERR experiments provide simultaneous structural, electronic and dynamic information not accessible by other techniques, they cannot afford a comprehensive picture of the processes at the molecular level.

In this work we have employed molecular dynamics (MD) simulations and electron pathways computations to characterize the structure, dynamics and ET properties of electrostatic Cyt/SAM complexes. The results allow for a sound interpretation of previous (spectro)electrochemical studies. Moreover, it is shown that conclusions derived from these simplified biomimetic systems may also hold for physiological ET complexes.

Computational Methods

System Setup. Initial Cyt structures were obtained from the PDB database, i.e. PDB 2GIW[26] for the reduced form (Cyt^{+2}) and PDB 1HRC[27] for the oxidized form (Cyt^{+3}). All MD simulations were performed using the AMBER package (Amber 2005), with the f99 force filed implementation.[28] The heme parameters were adopted from previous work.[29] To simulate the SAMs, an infinite array of fixed Au atoms with lattice structure 111 was built *in silico*. Each of the Au atoms was linked to a HS-$(CH_2)_5$-COOH (C_5) molecule through the S atom. SAM and lattice parameters were adopted from the literature.[30] The degree of ionization of the carboxyl-terminated SAMs was set to 10%, on the basis of previous experimental studies at pH 7 and within the relevant potential window.[31,32] The infinite array consists of a periodic boundary condition cell of 13 × 14 Au atoms in the *X*- and *Y*-directions, including the bound alkanethiols. In the *Z*-direction periodicity is achieved by using periodic boxes of 80 Å height, which leaves enough space between the Cyt surface and the next (upper) gold layer to avoid their direct interaction.

Binding of Cyt to the SAMs. Adsorption of Cyt to C_5-SAMs was investigated using steered MD (SMD).[33] For that purpose, 26 different configurations for each redox state (Cyt^{+3}, Cyt^{+2}) were generated with Cyt located at ∼5−10 Å away from the SAM surface. The 26 configurations differ in the rotational orientation of the protein with respect to the monolayer and were built by performing rigid body rotations of the Cyt structure. Starting from each configuration SMD were performed by pulling Cyt toward the monolayer at constant velocity, while computing the applied force. The pulling reaction coordinate (RC) is the distance between the central Au atom (which is fixed at the bottom of the SAM) and the center of mass of the Cα atoms of the protein. Integration of the force applied to move the protein toward the monolayer yields the work performed along the RC. In the SMD runs, the generalized Born model was used for implicit solvation.[34] Employing explicit water molecules was computationally too expensive due to the viscosity of the explicit solvent that imposes very low pulling speeds. The computed work-vs-RC plot can be taken as an estimate of the binding energy profile during the adsorption process. Although this is not a precise estimate of the free energy, it is useful for comparative purposes and allows identifying the possible structures of the Cyt/SAM complex. Typical work profiles obtained for nonbinding orientations show a steady increase in the values for the work while those profiles displaying possible binding orientations reveal the presence of a minimum in the profile at contact distance. All structures showing a minimum in the work-vs-RC profiles were selected as possible Cyt/SAM structures and subjected to explicit water PBC simulations as described below. This methodology has already been successfully applied to determine possible Cyt/SAM structure in our previous work.[25]

Binding Energy Calculations Using MM/PBSA. From the production MD simulations for each orientation of the protein, the

(14) El Kasmi, A.; Wallace, J. M.; Bowden, E. F.; Binet, S. M.; Linderman, R. J. *J. Am. Chem. Soc.* **1998**, *120*, 225.
(15) Feng, J. J.; Kuhlmann, U.; Murgida, D. H.; Utesch, T.; Mroginski, M.; Hildebrandt, P.; Weidinger, I. *J. Phys. Chem. B* **2008**, *112*, 15202.
(16) Kranich, A.; Naumann, H.; Molina-Heredia, F. P.; Moore, H. J.; Lee, T. R.; Lecomte, S.; de la Rosa, M. A.; Hildebrandt, P.; Murgida, D. H. *Phys. Chem. Chem. Phys.* **2009**, *11*, 7390.
(17) Murgida, D. H.; Hildebrandt, P. *J. Am. Chem. Soc.* **2001**, *123*, 4062–4068.
(18) Niki, K.; Hardy, W. R.; Hill, M. G.; Li, H.; Sprinkle, J. R.; Margoliash, E.; Fujita, K.; Tanimura, R.; Nakamura, N.; Ohno, H.; Richards, J. H.; Gray, H. B. *J. Phys. Chem. B* **2003**, *107*, 9947.
(19) Wei, J. J.; Liu, H. Y.; Khoshtariya, D. E.; Yamamoto, H.; Dick, A.; Waldeck, D. H. *Angew. Chem., Int. Ed.* **2002**, *41*, 4700.
(20) Xu, J. S.; Bowden, E. F. *J. Am. Chem. Soc.* **2006**, *128*, 6813.
(21) Yue, H. J.; Khoshtariya, D.; Waldeck, D. H.; Grochol, J.; Hildebrandt, P.; Murgida, D. H. *J. Phys. Chem. B* **2006**, *110*, 19906.
(22) Zuo, P.; Albrecht, T.; Barker, P. D.; Murgida, D. H.; Hildebrandt, P. *Phys. Chem. Chem. Phys.* **2009**, *11*, 7430.
(23) Murgida, D. H.; Hildebrandt, P. *J. Phys. Chem. B* **2002**, *106*, 12814.
(24) Kranich, A.; Ly, H. K.; Hildebrandt, P.; Murgida, D. H. *J. Am. Chem. Soc.* **2008**, *130*, 9844.
(25) Paggi, D. A.; Martin, D. F.; Kranich, A.; Hildebrandt, P.; Marti, M. A.; Murgida, D. H. *Electrochim. Acta* **2009**, *54*, 4963.
(26) Banci, L.; Bertini, I.; Huber, J. G.; Spyroulias, G. A.; Turano, P. *J. Biol. Inorg. Chem.* **1999**, *4*, 21.
(27) Bushnell, G. W.; Louie, G. V.; Brayer, G. D. *J. Mol. Biol.* **1990**, *214*, 585.
(28) Case, D. A.; Cheatham III, T. E.; Darden, T.; Gohlke, H.; Luo, R.; Merz, K. M., Jr.; Onufriev, A.; Simmerling, C.; Wang, B.; Woods, R. *J. Computat. Chem.* **2005**, *26*, 1668.
(29) Bikiel, D. E.; Boechi, L.; Capece, L.; Crespo, A.; De Biase, P. M.; Di Lella, S.; Lebrero, M. C. G.; Marti, M. A.; Nadra, A. D.; Perissinotti, L. L.; Scherlis, D. A.; Estrin, D. A. *Phys. Chem. Chem. Phys.* **2006**, *8*, 5611.
(30) Rai, B.; Sathish, P.; Malhotra, C. P.; Pradip; Ayappa, K. G. *Langmuir* **2004**, *20*, 3138.
(31) Murgida, D. H.; Hildebrandt, P. *J. Phys. Chem. B* **2001**, *105*, 1578.
(32) Ataka, K.; Heberle, J. *J. Am. Chem. Soc.* **2004**, *126*, 9445.
(33) Park, S.; Schulten, K. *J. Chem. Phys.* **2004**, *120*, 5946.
(34) Onufriev, A.; Bashford, D.; Case, D. A. *Proteins: Struct. Funct. Bioinf.* **2004**, *55*, 383.

Scheme 1. Representation of the Rotational Angles α (left) and φ (right)

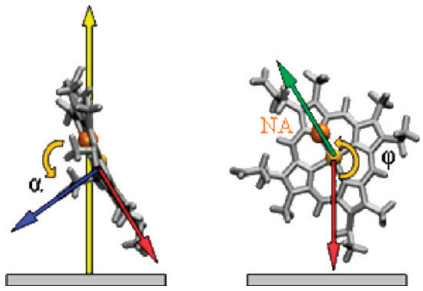

free energy of binding ΔG_B was calculated using MM/PBSA. The Cyt/SAM interaction energy in the gas phase (ΔE_{GAS}) is computed as the sum of electrostatic (ΔE_{ELEC}) and van der Waals (ΔE_{VDW}) contributions:

$$\Delta E_{GAS} = \Delta E_{ELEC+}\Delta E_{VDW} \quad (1)$$

The free energy of solvation (ΔG_{SV}) was estimated using the generalized Born implicit solvation method. Adding ΔE_{GAS} and ΔG_{SV} allows estimating ΔG_B.

For the sake of completeness, binding energies of Cyt^{+2} in a Cyt^{+3} preferential orientation and *vice versa* were calculated from four additional 25 ns MDs. These MDs with novel orientations for each redox state were also used when calculating every other parameter for Cyt^{+2} and Cyt^{+3}.

Explicit Water Simulations and Periodic Boundary Conditions. The production simulations of each complex were performed by immersing the Cyt/SAM structures obtained from the SMD simulations in a TIP3P water box, displaying an XY size corresponding to the 13 × 14 Au grid unit cell, and of 80 Å height. For each case an initial constant volume MD was performed to heat the system to 300 K, and subsequently a constant pressure simulation was performed to equilibrate the system density. Finally, the production MDs were performed. Temperature and pressure were kept constant using the Berendsen thermostat and barostat.[35] For the PBC simulations, Ewald summations were used to compute the electrostatic energy terms using the default parameters in the Sander module of the AMBER package.[28]

Characterization of the Cyt Orientation. The orientation of Cyt with respect to the Au/SAM surface is defined by the relative heme orientation using two angles. The angle α is given by the Fe−S(Met80) bond, which is perpendicular to the heme plane, and the *Z*-axis of the system which is perpendicular to the Au/SAM surface (Scheme 1). Values of α close to 0° or 180° imply that the heme lies parallel to the SAM, whereas values close to 90° indicate a heme orientation perpendicular to the surface. The second angle φ is defined by the Fe−N_A bond and the vector pointing toward the SAM which lies in the heme plane. This angle describes the rotational orientation of the heme and thus of the entire protein. Values between 0°−90° correspond to protein orientations with the propionate groups of the heme being closer to the SAM surface, whereas for values between 180°−270° the propionate groups are pointing away from the SAM surface.

It should be noted that for α values close to 0° or to 180°, changes of φ do not correspond to significant variations of protein orientation since the heme lies parallel to the monolayer surface. Therefore, for the purpose of a more intuitive representation that takes into account this effect, we have transformed φ according to

$$\varphi^* = \varphi\sqrt{1 - \left(\frac{\alpha - 90}{90}\right)^2} \quad (2)$$

In the corresponding plots shown in this work constant φ values are indicated as dotted isolines.

The protein dipole moment is computed with respect to the center of charge of the protein, as reported by Margoliash,[36] and its relative orientation is defined as the angle between the dipole vector and the *Z*-axis normal to the SAM plane.

Coupling Matrix Calculation. The electronic coupling between the entire heme group and any of the Au atoms that represent the electrode surface were estimated using the pathways algorithm developed by Beratan et al.[37,38] To obtain a proper description of the system, adjustments of the parameters of the pathways algorithm were required. First, all orbitals of heme iron were considered to be equivalent. Second, the coupling between the atoms of the heme was set equal to one in order to reproduce their resonant character. Finally, the coupling between each Au atom was set to one such that the results obtained to compute the electron pathway are independent of the Au atom of choice.

Results

Structural and Dynamical Characterization of Cyt/SAM Complexes. To select all possible Cyt/SAM complexes we applied the SMD protocol described above. Briefly, starting from many different rotational orientations of Cyt (for both the reduced and oxidized state) about 10 Å above the SAM, the protein was gently pulled toward the surface. To analyze the likeliness of the adsorption process for each orientation the work applied was measured as a function of Cyt/SAM distance. Unfavorable binding orientations show profiles for which the work increases steadily upon approaching of Cyt to the SAM surface, while those with favorable binding orientations display a minimum on the profile at contact distance (Figure S1 in Supporting Information). Seven favorable orientations were found for Cyt^{+3} and five for Cyt^{+2}, which are labeled as o1 to o7 and r1 to r5 respectively. For each of these plausible Cyt/SAM configurations, 20 ns MD simulations in explicit solvent were performed. The stability of the Cyt structure along the simulation was monitored by determining the rmsd with respect to the initial structure. The rmsd values are all below 2.5 Å indicating that the protein structure remains stable when adsorbed on the SAM and no partial denaturation occurs along the simulation.

The orientation of Cyt on the SAM surface is characterized by the angles α and φ, which describe the orientation of the heme group with respect to the SAM (vide supra). Figure 1A shows α-vs-φ* plots obtained for all the equilibrium simulations. In this plot each colored zone represents all the points obtained along each 20 ns simulation starting from one specific binding orientation of the protein in a given redox state.

Most of the orientations fall into a region denoted as main zone (MZ) with φ values close to 180°, and α values mainly around 100° but extending up to 160°. These conformations correspond to Cyt with the lysine patch around the exposed heme edge facing the SAM. Values of φ close to 180° indicate that heme propionates tend to point away from the SAM surface. Within the MZ there is a significant population of conformations with α very close to 90°, i.e. with the heme group oriented

(35) Berendsen, H. J. C.; Postma, J. P. M.; Vangunsteren, W. F.; Dinola, A.; Haak, J. R. *J. Chem. Phys.* **1984**, *81*, 3684.
(36) Koppenol, W. H.; Rush, J. D.; Mills, J. D.; Margoliash, E. *Mol. Biol. Evol.* **1991**, *8*, 545.
(37) Beratan, D. N.; Onuchic, J. N.; Betts, J. N.; Bowler, B. E.; Gray, H. B. *J. Am. Chem. Soc.* **1990**, *112*, 7915.
(38) Beratan, D. N.; Onuchic, J. N.; Winkler, J. R.; Gray, H. B. *Science* **1992**, *258*, 1740.

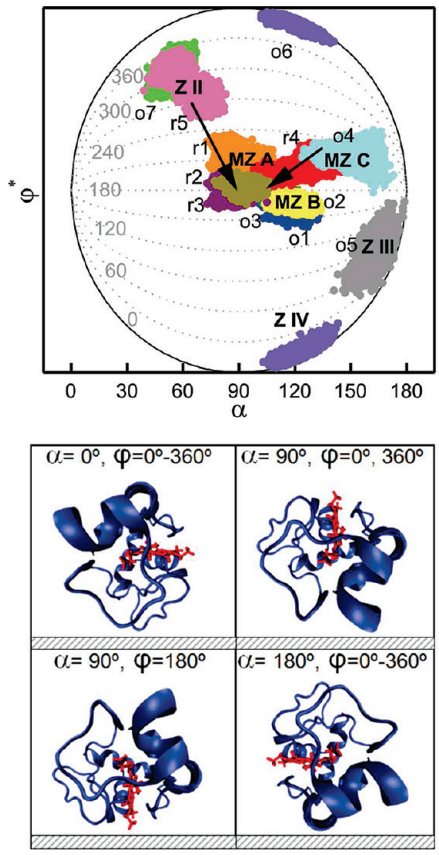

Figure 1. Top: α-vs-φ* plots for all equilibrium MD simulations in explicit water. Each point represents a snapshot from the corresponding MD. Snapshots were taken every 10 ps. Arrows indicate global rotations of the protein along the simulation. Plots labeled by "o" and "r" refer to oxidized and reduced Cyt, respectively. The dotted lines represent isovalues of φ. For an α-vs-φ plot see Figure S2 in Supporting Information. Bottom: Schematic representation of Cyt orientation at extreme α and φ values. The SAM is represented by the dashed areas. Note that for α = 0° and α = 180° different φ values do not represent different protein orientations

perpendicular to the SAM surface. In this region the mean dipole moment is high (∼570 D), with a mean angle with respect to the *Z*-axis of 152°. A closer look to the MZ shows that three subzones can be defined: MZC that exhibits the highest α values and comprises o4 and a part of r4; MZB defined by o1, o2 and o3; and MZA represented by r1, r2 and r3.

Three other zones can be defined: zone II (r5 and o7), characterized by a heme plane tilted by about 50° with respect to the surface and a very low protein mean dipole (∼250 D); zone III (o5), with the heme nearly parallel to the surface; and zone IV (o6) with the heme tilted about 40° with respect to the surface but on the opposite side of zone II. Zones III and IV show intermediate protein dipole values of about 430 D with angles with respect to the normal of 140° and 133°, respectively.

Note that, given the asymmetry of the heme location inside the protein fold, different orientations define different distances between the heme-iron and the SAM surface. In the MZ Cyt lies with the heme facing the SAM, and thus, the iron−SAM distance is about 10−12 Å. In the other zones the heme is more remote from the surface with distances increasing above 16 Å.

An interesting conclusion that can be derived from Figure 1 is that, although the rotation of the adsorbed protein is obviously restricted with respect to solution, it still exhibits significant mobility, as inferred from the range of α and φ values that are explored for each starting conformation. In most cases the protein remains adsorbed roughly by the same surface patch (i.e. with the same coarse orientation) during the simulation time, but in some other cases the molecules rotate by more than 20°, thereby changing significantly the orientation and contact surface. These reorientations are accompanied by small structural changes of the protein that may have an impact on its redox properties (vide infra). The arrows in Figure 1A provide a rough indication of the net direction of the large amplitude motion (initial vs final) of Cyt along the dynamics for ZII, MZA and MZC. It can be seen that for these starting configurations Cyt rolls over the SAM exploring a broad range of orientations represented by the colored areas, but it finally tends toward the central zone of the plot. Although less clear due to the smaller total area, a similar observation is made for MZB. This behavior suggests that the complete orientational space might be described by the sum of the different simulations and that, in those cases where the areas overlap, the movement from one conformation to the other might be possible, although it cannot be captured by the simulations due to time constraints inherent to the method.

Binding Energies for the Different Domains. To further characterize the Cyt/SAM complexes, we have computed the potential energy surface of the binding process along all trajectories using the MM/PBSA approximation, as described in the Computational Methods section. The mean values of the binding energies obtained for each simulation are summarized in Table S3 in the Supporting Information, along with the different contributions to the total energies. All conformations exhibit relatively high binding energies dominated by electrostatic contributions which are partially compensated by changes of the solvation free energy. As expected, the lower binding energies correspond to the initial protein configurations that exhibit higher mobility, with r4 and r5 being the most mobile ones. In contrast, MZ exhibits the higher binding energies, as well as the largest dipole moments perpendicularly oriented with respect to the surface and, therefore, is considered the preferred adsorption domain.

A closer look at the MD simulations and binding energies related to the MZ indicate two distinctive clusters that correspond to different redox states. Cyt^{+2} is likely to be found in MZA, while Cyt^{+3} is preferentially found in MZB. The differences are highlighted in Figure 2 by plotting the binding energy of both redox states as a function of the orientation for all simulations in the MZ. For Cyt^{+2} we can identify two energy wells at (α = 90°, φ = 180°) and (α = 105°, φ = 145°) separated by a small barrier. In contrast, Cyt^{+3} shows a deeper minimum at (α = 130°, φ = 160°) and a slightly higher second well at (α = 115°, φ = 190°). The existence of multiple energy wells and the differences between redox states indicate that Cyt binding is not homogeneous and multiple orientations may coexist in thermal equilibrium. In agreement with this prediction, Araci et al. have reported a distribution of orientations for Cyt adsorbed on indium−tin oxide, with preferential orientations corresponding to α ≈ 50°.[39] Note that this tilt angle is indistinguishable from α = 130° according to our orientation characterization.

In order to verify the redox state dependence of the orientation, four additional 25 ns MD simulations were performed by placing the structure of Cyt^{+2} in orientations typical for Cyt^{+3} and *vice versa*. In all cases the simulations resulted in a reorientation of the protein molecules toward the configurations

(39) Araci, Z. O.; Runge, A. F.; Doherty III, W. J.; Saavedra, S. S. *J. Am. Chem. Soc.* **2008**, *130*, 1572.

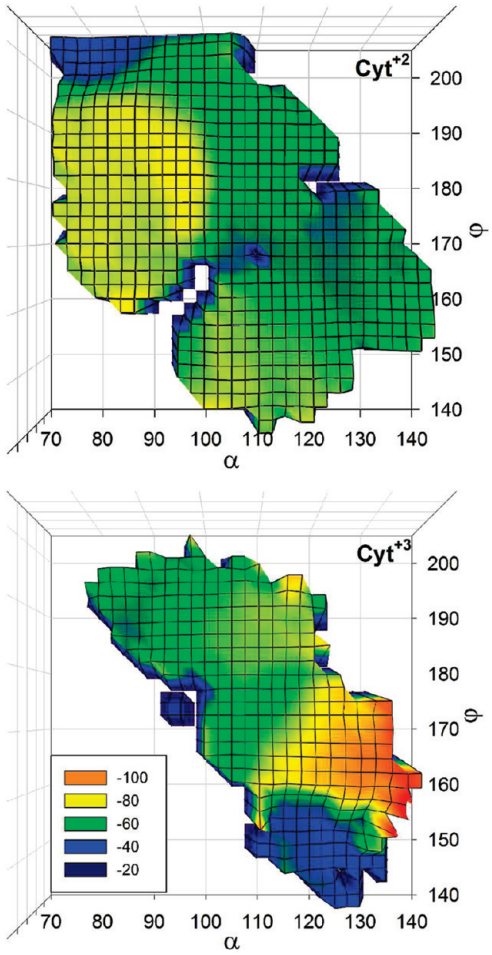

Figure 2. Binding energy vs orientational angles for the reduced (top panel) and oxidized (bottom panel) Cyt. The color code indicates increasing binding energies from -20 kcal mol^{-1} (blue) to -100 kcal mol^{-1} (red).

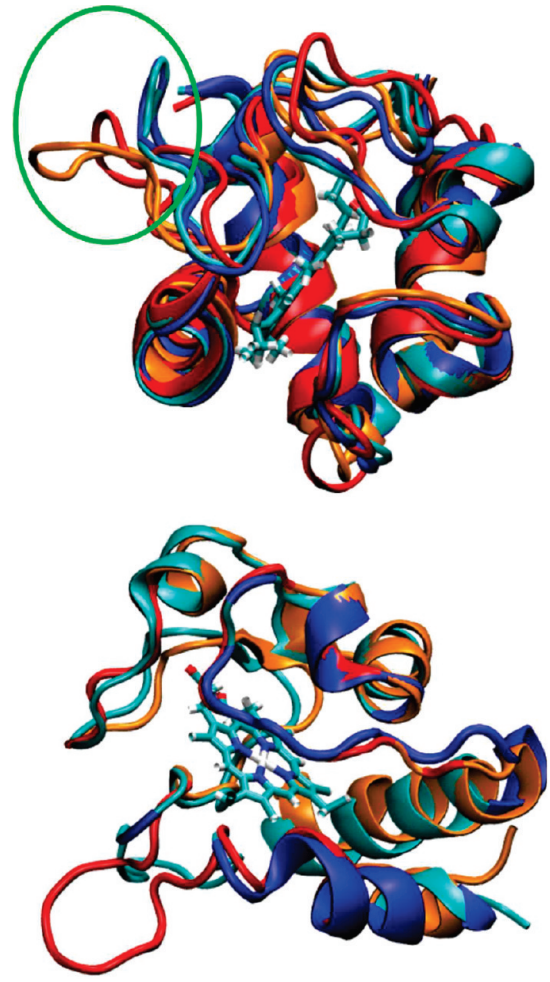

Figure 3. Top: comparison of MD average structures for oxidized (cyan) and reduced (orange) Cyt, together with the crystallographic structures of the oxidized (blue) and reduced (red) Cyt. The green circle indicates the αAβ1 loop. Bottom: SAM binding zone highlighted on the reduced (orange-red) and oxidized (blue-cyan) structures. SAM contact zones are represented in red and blue for Cyt^{+2} and Cyt^{+3}, respectively.

preferred in the respective redox state. Therefore, the redox state dependence of the protein orientation displayed in Figure 2 cannot be ascribed to improper sampling.

Structural Determinants of (Differential) Binding. In order to understand the structural basis for the differential adsorption of Cyt^{+2} and Cyt^{+3}, we have analyzed the different structures obtained by MD simulations in comparison to the corresponding crystallographic structures. First, we have compared average structures for all simulations of Cyt^{+2} and Cyt^{+3} in the MZ (A and B) using both the crystallographic and the average structures as a reference. As shown in Figure S4 and Table S5 in the Supporting Information, no significant structural differences are observed between structures of different simulations showing that each redox state is in a stable conformation. Figure 3 shows two selected average structures (one for each redox state) together with the initial X-ray structures.[26,27]

The main difference between the structures is located in the αAβ1 loop. For Cyt^{+3} the average structure remains very similar to the crystallographic structure, and they are clearly different from those of Cyt^{+2}. Comparison of rmsd values for the entire protein and the loop only (Table S5 in the Supporting Information) shows that for Cyt^{+3} the loop exhibits mobility comparable to the whole protein, and furthermore, the structure remains very close to the crystallographic one. Also for Cyt^{+2} the mobilities of the loop and of the whole protein are very comparable. However, in this case the establishment of contacts between the loop and the SAM induces a larger structural distortion of the loop with respect to the starting crystal structure. Analysis of the interaction zones with the SAM surface explains these differences (Figure 3). Both redox states bind through the C-terminal helix A (lysine13), the αDE or ω loop (lysines 79, 86 and 87) and the small helix D (lysines 72, 73). In the reduced state, however, additional interactions are formed with lysines 22 and 25 from the αAβ1 loop, forcing the loop to adopt the observed conformation and rotating the molecule to lower α values. In the oxidized state, on the other hand, a new contact is established with Lys8 located at the beginning of helix A, thus forcing the molecule to rotate toward higher α values.

Note that the computationally predicted Cyt^{+3} contact lysines are in excellent agreement with previous experimental observations by Xu et al.[20]

Analysis of Electronic Couplings. To analyze the influence of protein dynamics and the different binding orientations on the heterogeneous ET reaction, we have computed the optimum electron pathways and their corresponding electronic coupling matrices (T_{DA}) along the simulations for each of the Cyt/SAM complexes described above using the pathways algorithm. The results summarized in Table 1 show that couplings strongly depend on the orientation and binding zone. The highest average

Table 1. Electronic Coupling Calculations Using the Pathways Algorithm (all values are expressed in eV)[a]

MD	zone	$\langle T_{DA} \rangle$	T_{DA}^{Min}	T_{DA}^{Max}	[b]optimal path
r1	MZ A	4.59×10^{-4}	5.81×10^{-5}	1.85×10^{-3}	HEM-CYS17-SAM
r2	MZ A	4.4×10^{-4}	8.32×10^{-5}	1.4×10^{-3}	HEM-CYS17-SAM
r3	MZ A	5.1×10^{-4}	1.72×10^{-4}	1.7×10^{-3}	HEM-CYS17-SAM
o1/r	MZ A	5.25×10^{-4}	8.79×10^{-5}	1.6×10^{-3}	HEM-SAM
o3/r	MZ A	3.24×10^{-4}	7.25×10^{-5}	9.37×10^{-4}	HEM-SAM
o3	MZ B	4.2×10^{-4}	1.16×10^{-4}	1.7×10^{-3}	HEM-SAM
o2	MZ B	8.02×10^{-5}	2.57×10^{-5}	2.53×10^{-4}	HEM-WAT-SAM
o1	MZ B	6.9×10^{-5}	8.83×10^{-6}	3.7×10^{-4}	HEM-WAT-SAM
r2/o	MZ B	2.7×10^{-4}	6.87×10^{-5}	9.3×10^{-4}	HEM-SAM
r3/o	MZ B	1.25×10^{-5}	2.73×10^{-6}	6.01×10^{-5}	HEM-SAM
r4	MZ B/C	9.8×10^{-5}	1.28×10^{-5}	4.8×10^{-4}	HEM-SAM
o4	MZ C	2.1×10^{-5}	3.57×10^{-6}	1.1×10^{-4}	HEM-MET80-LYS79-SAM
o7	II	7×10^{-6}	1.52×10^{-6}	3×10^{-5}	HEM-ARG38-SAM
r5	II	8.5×10^{-6}	1.94×10^{-6}	3.7×10^{-5}	HEM-GLY41-SAM
o5	III	8×10^{-7}	3.24×10^{-7}	2.31×10^{-6}	HEM-MET80-WAT-SAM
o6	IV	1.1×10^{-6}	5.65×10^{-7}	2.32×10^{-6}	HEM-TRP59-THR58-SAM

[a] Labels "o" and "r" refer to oxidized and reduced Cyt, respectively (see Figure 1A and corresponding text). The o#/r label denotes a Cyt^{+3} structure in a starting orientation that correspondes to Cyt^{+2} preferential binding and *vice versa* for r#/o. $\langle T_{DA} \rangle$, $T_{DA}^{Min}$and T_{DA}^{Max} stand for average, minimum and maximum coupling, respectively. [b] For optimal paths belonging to MZ A and MZ B, HEM stands for the pyrrolic ring C.

and maximum couplings ($\langle T_{DA} \rangle$ and T_{DA}^{Max}, respectively) are observed in the MZ, particularly MZA. Zones II, III and IV exhibit $\langle T_{DA} \rangle$ values that are 2−3 orders of magnitude lower than in the MZA, and therefore, these configurations are unlikely to be relevant for the heterogeneous ET reaction.

The dependence of T_{DA} on α and φ in the MZ is shown in Figure 4. For both Cyt^{+2} and Cyt^{+3}, maximum couplings are achieved at angles of $\alpha \approx 90°$ and $\varphi \approx 195°$, which correspond to the heme group nearly perpendicular to the surface and in direct contact to the SAM. A comparison of Figures 2 and 4 reveals that for Cyt^{+2} the optimum orientation in terms of T_{DA} is relatively close to the maximum of the binding energy. Thus, establishing maximum coupling for the thermodynamically most stable orientation requires a relatively small rotation (∼20°) with respect to φ. For Cyt^{+3}, in contrast, the best binding subzone corresponds to low coupling values, while the high-coupling zone shows weak binding. Therefore, Cyt^{+3} binds preferentially trough a low-coupling zone, thus requiring a large amplitude reorientation (40−50° in each angle) to achieve maximum coupling. This may result in protein movement being the rate-limiting event in the reduction of Cyt^{+3}, consistent with experimental observations.[24]

Structural Analysis of ET Paths. The present results clearly show that the protein orientation determines the order of magnitude of the T_{DA}. A detailed analysis of calculated T_{DA} values along the MD simulations shows that, in addition to the coarse orientation effect described above, small structural fluctuations may alter T_{DA} values by up to 1 order of magnitude, thus exerting a fine-tuning of the ET rate. The molecular basis of such tuning resides in low-amplitude global breathing motions of the protein and the mobility of interfacial water molecules. The first effect is exemplified in Figure 5 for one simulation of Cyt^{+2} in the MZ. It can be seen that small fluctuations of the heme group and side chains of a properly oriented molecule are sufficient for varying T_{DA} by a factor of 3−5, corresponding to alterations of k_{ET} by a factor of 9−25.

In addition, water molecules can transiently turn a low-coupling pathway into a more favorable one, by bridging through-space jumps and converting them to tightly coupled hydrogen-bond mediated ones. This is shown in Figure 6 for one MD simulation of Cyt^{+3} in the MZ. The spikes that represent 10-fold increases of T_{DA} do not correlate with orientational changes, but are caused by transient short-circuiting of the pre-established pathway by water molecules.

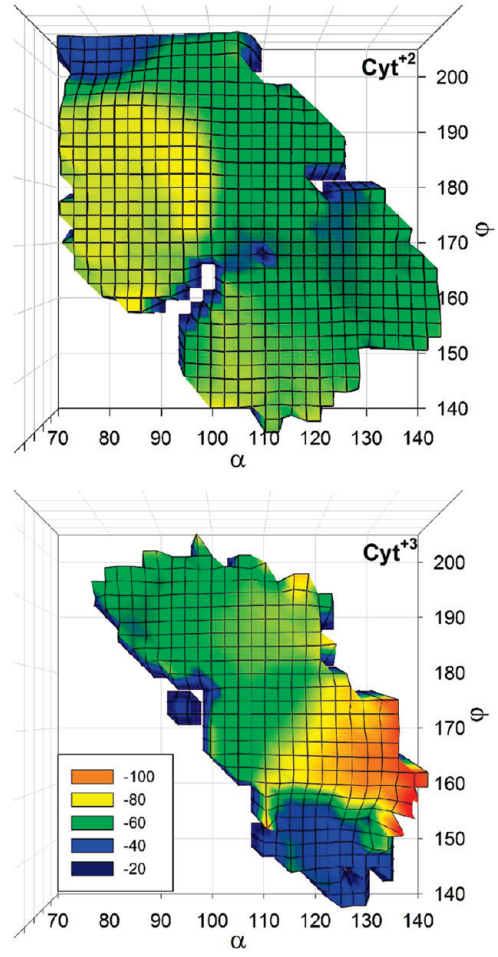

Figure 4. Average electronic couplings as a function of the orientational angles for the reduced (top panel) and oxidized (bottom panel) Cyt. The color code indicates increasing electronic couplings from 0.2 meV (blue) to 0.8 meV (orange).

Note that protein, water, and SAM mobility, which are crucial for the fine-tuning of the T_{DA}, are likely to be affected by the temperature, viscosity and electric field strength at the interface. In the present simulations the electrode potential and, therefore, the interfacial electric field, is not explicitly considered. It is very likely that under the influence of the strong electric fields

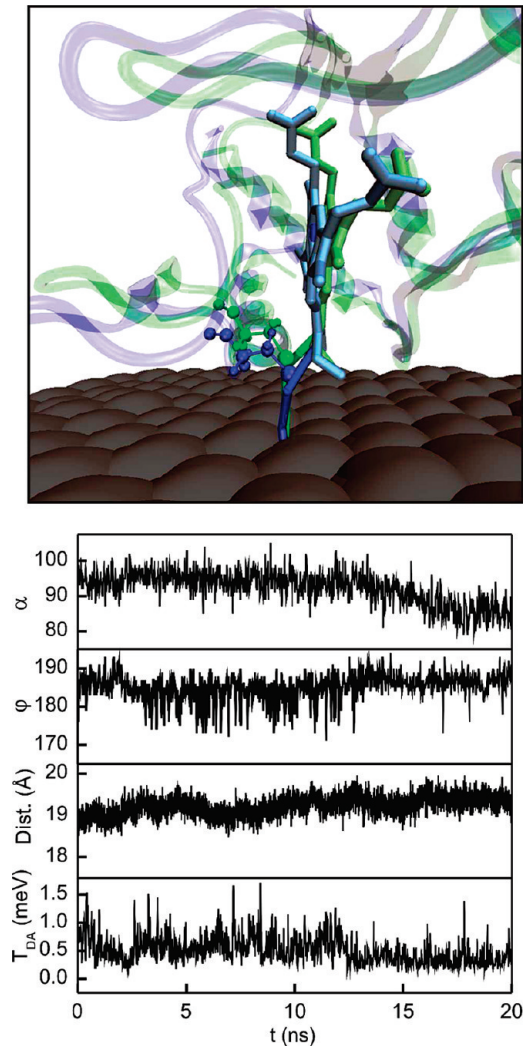

Figure 5. Variations of the electronic coupling due to heme and heme side chain fluctuations. The bottom panel shows the variations of the angles α and φ, the distance from the heme iron to the Au and the electronic coupling along the 20 ns simulation. The blue vs green structures represent a configurational change associated with a 2−5-fold increase in the electronic coupling.

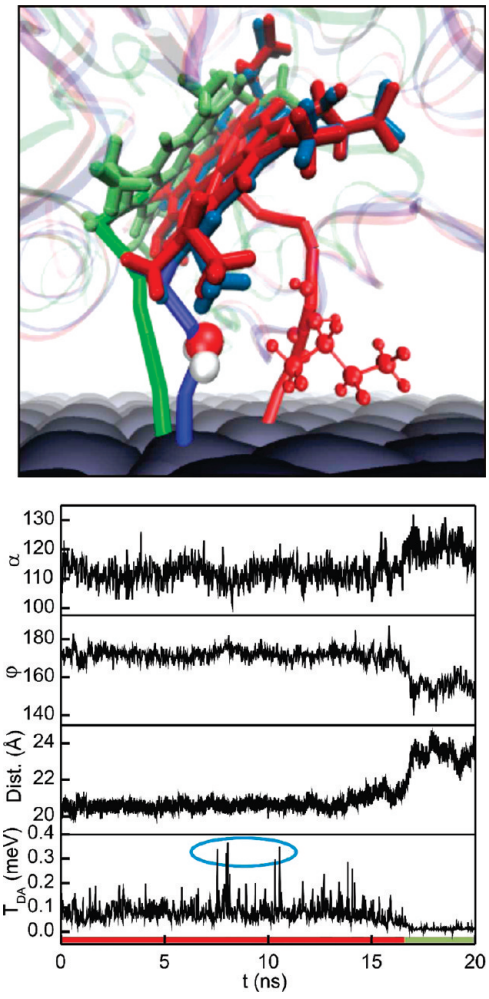

Figure 6. Water-mediated increase of the electronic coupling. The top panel represents different electronic pathways in different colors. Red: optimum pathway involving a through-space jump. Blue: pathway short-circuited by water molecules. Green: pathway after reorientation of Cyt with an increased heme−SAM distance. The bottom panel shows the variations of the angles α and φ, the distance from the heme iron to the Au and the electronic coupling along the 20 ns simulation. The color code is similar to the one employed in the top panel and indicates the optimal pathways operating along the simulation.

characteristic of electrochemical and biological interfaces the mobility is largely restricted, and consequently, the most favorable configurations might be reached with lower frequency. On the other hand, it can be expected that the lifetime of the favorable configurations is also extended considerably, thus increasing the probability of electron tunnelling from such configurations.

Dynamical Analysis of Cyt Dipole. As shown above, Cyt achieves maximum dipole moment values within the MZ. A closer look reveals that the modulus and direction of the dipole vary significantly along the simulations (Figures S6 and S7 in the Supporting Information). Variations of the modulus mainly arise from the movement of charged residues during the MD, while the direction varies in response to both the movement of charged residues and concerted rotations of the protein. This effect is visualized in Figures 7 and 8 for both Cyt^{+2} and Cyt^{+3}.

For Cyt^{+2} two regions of high and low dipole moment values can be clearly distinguished. Maximal dipole moments are found at two locations: ($\alpha = 80°$, $\varphi = 185°$) and ($\alpha = 120°$, $\varphi = 200°$), i.e. with the heme propionates pointing away from the SAM. Interestingly, dipole moment orientations close to 180° (i.e., perpendicular to the surface) are achieved in two zones which overlap with those of the highest dipole moment values. In contrast, Cyt^{+3}, which generally displays lower dipole moment values, does not show any evident correlation between modulus and direction. Note that for Cyt^{+3} the variations of the dipole modulus are much smaller than for Cyt^{+2}. The differences can be mainly ascribed to the enhanced structural flexibility of Cyt^{+2} upon contacting the αAβ1 loop with the SAM (see above). The magnitude of the change of the dipole moment is in agreement with previous studies showing that subtle deformations of Cyt that do not represent a change of secondary structure may induce significant variations of this parameter.[40]

Finally, it is interesting to compare binding energies (Figure 2) and dipole moments (Figures 7 and 8). In the present work all simulations have been performed considering an uncharged metal substrate that is not subjected to an externally applied potential.

(40) De Biase, P. M.; Paggi, D. A.; Doctorovich, F.; Hildebrandt, P.; Estrin, D. A.; Murgida, D. H.; Marti, M. A. *J. Am. Chem. Soc.* **2009**, *131*, 16248.

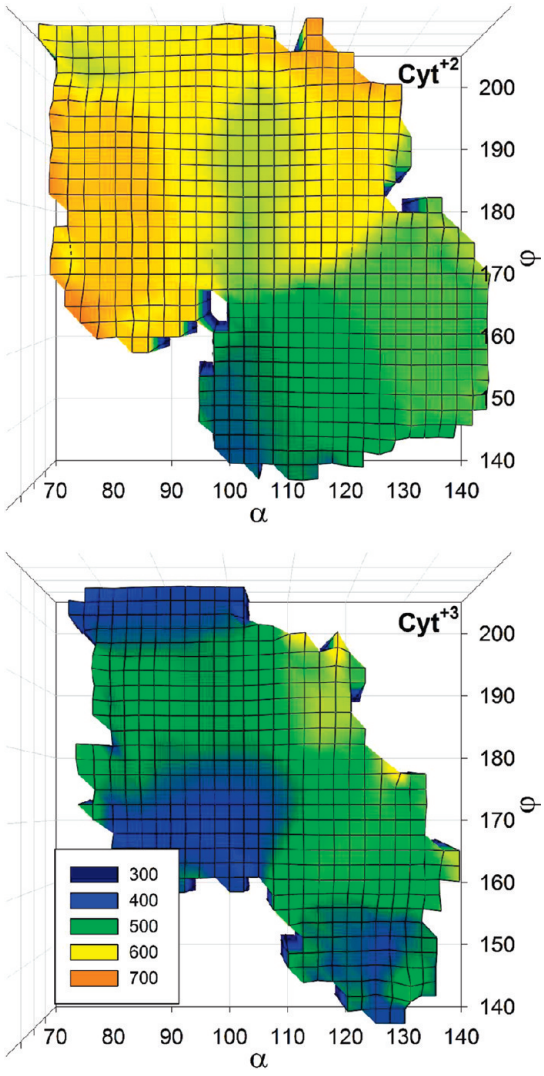

Figure 7. Total protein dipole moment as a function of the orientation for reduced (top panel) and oxidized (bottom panel) Cyt. The color code indicates increasing dipole moments from 300 D (blue) to 700 D (orange).

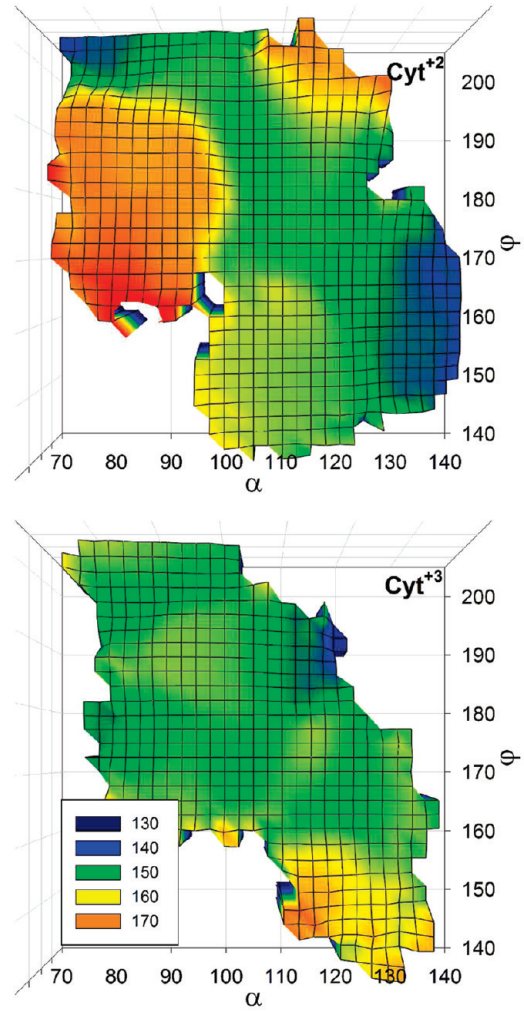

Figure 8. Dipole moment orientation as a function of the protein orientation for the reduced (top panel) and oxidized (bottom panel) Cyt. The color code indicates increasing perpendicularity of the dipole moment with respect to the Au surface from 130° (blue) to 170° D (orange).

Thus, from the point of view of the charges only, this situation is comparable to a working electrode close to its potential of zero charge (E_{pzc}). In the experimental studies performed on equivalent systems, however, potentials may be well above or below E_{pzc}, depending on the nature of the metal and the coating. This implies that the adsorbed Cyt molecules experience strong interfacial electric fields (E_F) that can affect the protein orientation significantly. The E_F will favor those orientations with the dipole perpendicular to the surface (i.e., parallel to the E_F vector). Therefore, the total Cyt/SAM interaction energy will be a combination of the binding energies calculated in the absence of an E_F and the interactions of the E_F with the dipole moment. In a first approach, the result can be considered as an E_F-weighted combination of the plots in Figures 2, 7 and 8. In the low E_F regime, the protein is expected to be preferentially oriented according to the minima in Figure 2. In contrast, high E_F values will drive the protein to the maxima of Figure 8.

Discussion

What Governs Cyt Orientation? The results presented in this work have several implications concerning the orientation of Cyt in electrostatic complexes with carboxyl-terminated SAMs. First, the existence of multiple energy wells suggests a distribution of orientations of the adsorbed proteins. Second, the adsorbed molecules exhibit significant mobility that can be described as protein rotations on the surface driven by the formation of new lysine/SAM interactions and the concomitant losing of other contacts. Third, binding energy analysis shows that Cyt^{+2} and Cyt^{+3} have different preferred orientations due to small structural variations at the level of the αAβ1 loop.

These conclusions are valid for an uncharged metal substrate. At an electrochemical interface the preferred orientation will depend not only on the specific protein/SAM interactions but also on the unspecific interactions of the protein dipole moment with the interfacial E_F. Given that dipole moment orientations and binding energy surfaces show different optimum distributions (Figures 2 and 8), their relative populations are expected to respond to changes of the applied potential. This prediction is in very good agreement with previous experimental results which show a change in the average heme orientation as function of the E_F controlled either by the electrode potential, the SAM thickness or the solution pH.[24,25]

What Determines the Observed ET Rate? Long-range ET kinetics can be described in terms of the high-temperature limit of Marcus semiclassical equation, which can be expressed as the product of a Franck−Condon (FC) factor and the T_{DA} term.

The FC factor is determined by the reorganization energy (λ) and by $\Delta G°$, which in turn depends on the standard reduction potential of Cyt ($E°$). Neither λ nor $E°$ is expected to be a function of the protein orientation, unless different orientations produce significant alterations of the protein structure to different extents. As shown in previous sections, MD simulations only detect minor structural variations at the level of the $\alpha A\beta 1$ loop but not at the level of the heme, and only for Cyt^{+2}. Therefore, variations of k_{ET} can be primarily assigned to differences in T_{DA} for different orientations.

Pathways computations along MD simulations of the Cyt/SAM complexes show that optimal T_{DA} values strongly depend on the protein orientation. Indeed, relatively small reorientations of the complexes within the MZ result in changes of T_{DA} by a factor of 2−10, which corresponds to a 4−100 fold variation of the heterogeneous k_{ET}. Moreover, orientations with the best electronic coupling do not overlap with those exhibiting the highest binding energies and/or optimum E_F−dipole alignments, as also observed experimentally for Cyt adsorbed on indium−tin oxide.[39] Therefore, on the basis of the present results, the following scenario can be envisaged for an electrochemical experiment.

Given an orientational ensemble, proteins in orientations of best electronic coupling will be reduced/oxidized first, resulting in a modified ensemble that will relax to the corresponding equilibrium distribution. This ET-coupled reorientation is driven by the different energy and dipole distributions obtained for each redox state. In the presence of a strong E_F two effects are expected to modify the ET rate. First, the E_F will change the orientational distribution by favoring those orientations with an aligned dipole. The resulting ensemble is expected to have lower $\langle T_{DA} \rangle$ values, i.e. lower measured k_{ET}, since best couplings values do not correspond to an E_F aligned dipole. Second, reorientation of the protein to a more favorable conformation for ET is expected to be retarded in the presence of a strong E_F due to dipole alignment. The magnitude of the latter effect can be estimated based on the orientation-dependence of the binding energy, coupling and dipole moment. Assuming that the orientational population of Cyt is determined only by the binding energy, a Boltzmann analysis shows that Cyt^{+2} presents significant populations only for α values between 90°−100° (see Figure S8 in the Supporting Information), i.e. similar to the values for α that represent the best couplings in this redox state. However, in order to achieve maximum coupling, the protein needs to rotate by ∼30° in the φ direction. Such a rotation would imply an activation energy (E_a) of ∼16 kcal·mol^{-1}, estimated as the difference between the binding energy in the preferred orientation and the maximum energy found along the motion toward the target orientation, i.e. the one with highest electronic coupling. Cyt^{+3}, on the other hand, presents a narrower distribution, localized around $\alpha = 130°$ and $\varphi = 155°$. Thus, in order to reach the highest coupling zone, Cyt^{+3} must rotate 30° in each angle, which implies $E_a \approx 40$ kcal·mol^{-1}.

In the presence of a homogeneous E_F, the activation energy required for rotation of Cyt from the best binding zone to the best coupling zone includes an additional work term

$$W_{EF} = -|\vec{\mu}| \cdot |\vec{E}_F| \cos\theta \qquad (3)$$

where $\vec{\mu}$ is the permanent dipole moment, $|\vec{E}_F|$ is the electric field and θ is the angle between $\vec{\mu}$ and $|\vec{E}_F|$. Table 2 shows the effect of this additional activation term on k_R estimated for different field strengths assuming an Arrhenius-like behavior.

Table 2. Estimation of the E_F Effect on k_R of Cyt^{+2} and Cyt^{+3} for the Transition from the Most Stable Orientation to the One Providing Optimal Electronic Coupling

E_F (V·Å^{-1})	W_{EF} (kJ·mol^{-1})	E_a (kJ·mol^{-1})	$k_R/k_{R/EF}$
	Cyt^{+3}		
0	0	167.5	1
0.001	1.4	168.9	0.6
0.01	14.0	181.5	3×10^{-3}
0.05	70.0	237.4	5.5×10^{-13}
0.1	139.9	307.3	3.0×10^{-25}
1	1398.7	1566.1	6.7×10^{-246}
	Cyt^{+2}		
0	0	67.3	1
0.001	0.6	67.9	0.8
0.01	6.4	73.7	7.6×10^{-2}
0.05	31.8	99.1	2.6×10^{-6}
0.1	63.7	131.0	6.9×10^{-12}
1	636.7	704.0	2.4×10^{-112}

As expected, moderate fields comparable to those expected at electrochemical and biological membrane interfaces may have a drastic effect on k_R.

Electric fields are not only expected to influence the coarse orientation and activation barriers for reorientation of Cyt in the electrostatic complexes. Small thermal fluctuations of the adsorbed protein and interfacial water molecules, which have been shown here to be crucial for establishing transient ET paths of high T_{DA}, should also be slowed down significantly in the presence of sufficiently strong fields. The result would be a reduced probability of reaching configurations of best electronic couplings and, therefore, a lower apparent ET rate.

The present results provide a consistent molecular interpretation to the distance-dependence of the apparent ET rates observed experimentally for Cyt and other proteins on SAM-coated electrodes. At thick SAMs the E_F at the protein binding site is small and, therefore, protein and interfacial water molecules are able to experience fast reorientation. In this regime the distance between the electrode and the redox center implies low T_{DA} values and, thus, electron tunnelling is the rate limiting event. At thinner films the interfacial E_F increases, thereby retarding reorientation and thermal fluctuations that, hence, become rate-limiting.

Physiological Relevance of the Biomimetic Complexes. SAM-coated electrodes have been extensively employed for investigating redox proteins. There is no doubt that these biocompatible systems represent a powerful platform for performing electrochemical and spectroelectrochemical studies that can afford valuable thermodynamic, kinetic and structural information of the immobilized protein. In some cases they can also be regarded as biomimetic in the sense that they reproduce some basic features of the physiologically relevant interface. The question whether conclusions derived from experiments with such simplified biomimetic systems can be extrapolated to real complexes, however, remains unanswered. In the specific case of Cyt/SAM complexes, the first issue to be considered is their structural/orientational correlation with the physiological complexes of Cyt with mitochondrial membrane complexes III and IV (bc_1 and CcO, respectively). Regrettably, there is no available crystal structure for any of the corresponding mammalian protein−protein complexes, although a structural model for the mammalian Cyt/cytochrome *c* peroxidase (Cyt/CcP) complex has been proposed.[41] The structure of the complex of yeast *iso-*

(41) Pelletier, H.; Kraut, J. *Science* **1992**, *258*, 1748.

Table 3. Observed Electrostatic Cyt/partner Interactions

Complex			
Cyt/bc_1	Cyt/CcO	Cyt/CcP	Cyt/SAM
−	Lys8	Lys5	Lys8
Lys13	Lys13	Lys13	Lys13
Lys27	Lys72	Lys72	Lys72
Lys79	Lys73	Lys73	Lys73
Lys86	Lys86	Lys86	Lys86
Lys87	Lys87	Lys87	Lys87

Cyt with bc_1 has also been reported.[42] Thus, a crude estimate of the possible electrostatic contacts in the equivalent mammalian complex can be obtained by superimposing the structure of horse heart Cyt with the available *iso*-Cyt/bc_1 complex structure. For Cyt/CcO complexes, on the other hand, no structure is available for any species, but the interactions have been simulated using a rigid docking approach.[43] The analysis of the three model complexes (Cyt/CcP; Cyt/bc_1 and Cyt/CcO) indicates that the electrostatic interactions of Cyt with any of the partners rely on 5−6 Lys residues which are essentially the same in all cases (see Table 3). Interestingly, the Cyt/SAM system mimics correctly the putative binding mode of Cyt to CcO and CcP, and also reproduces 3 out 5 predicted Cyt/bc_1 interactions.

According to the results of the present work, maximum T_{DA} values are obtained by direct contact of the heme edge with the SAM surface. This conclusion agrees with a previous proposal for the optimal electron pathway from Cyt to CcO. The predictions of MD simulations on Cyt/SAM biomimetic systems are also in agreement with previous experimental results indicating differential adsorption of Cyt^{+2} and Cyt^{+3} to CcO, as well as rearrangements of the complex upon interprotein ET.[44−47] Moreover, it has been shown that increasing transmembrane potentials slow down the catalytic activity of CcO toward Cyt.[48,49] In the same line, the reaction between Cyt and CcP is inhibited at low ionic strengths, presumably due to electrostatic freezing of the interprotein complex.[50] Bell-shaped-behaved ionic strength dependencies of the ET rates have also been observed for other interprotein redox complexes,[51−54] and can be generally interpreted in terms of the qualitative picture emerging from the present simulations.

Thus, it appears that the Cyt/SAM complexes studied here by computational methods and experimentally in previous work are able to reproduce some essential features of the physiological complexes and, at the same time, exhibit the simplicity required for in-depth physicochemical studies.

Conclusions

The simulations presented here refer to a simplified system where the high local electric field present at electrochemical and biological interfaces are not explicitly considered. Under these conditions, it is shown that even for Cyt which is regarded as the typical example of a redox protein possessing a well-defined charged binding site, electrostatic interactions with an oppositely charged model system lead to a distribution of orientations and, therefore, to a distribution of electron tunnelling probabilities. Moreover, it is shown that the adsorbed protein exhibits significant mobility in the electrostatic complex. These results suggest that the measured ET rates in real complexes represent a convolution of orientational dynamics and tunnelling probabilities. Moreover, subtle structural fluctuations of the protein and interfacial water molecules that do not imply coarse reorientation can be sufficient for modulating the ET rate by more than 2 orders of magnitude.

Certainly much more work with model systems of higher complexity is required for a precise description that can be quantitatively compared with real systems. The simplified system, however, captures the essence of the problem and provides a molecular picture that qualitatively should also hold for real complexes. The essential difference that can be anticipated is a narrower distribution of orientations and lower protein and interfacial water mobility due to the action of the interfacial electric fields and possible specific interactions. This effect might be at the origin of the "unusual" distance-dependence of the ET rates experimentally observed for a variety of proteins in similar systems, which has been a long-standing open question in bioelectrochemistry.

Moreover, the findings from the present computational study may have important implications for the *in vivo* control of ET processes in the respiratory chain, particularly related to the possible modulation by the transmembrane potential,[5,40] and provide a consistent molecular picture for the widely observed bell-shaped dependence of ET kinetics with ionic strength in protein−protein redox complexes.[50−54]

Acknowledgment. Financial support by ANPCyT (PICT 2006-459, 2007-314 and 2007-650), UBA (08-X625), and the DFG (Cluster of Excellence) is gratefully acknowledged. Computer simulations were done using resources kindly provided by the Open Science Grid, which is supported by the National Science Foundation and the U.S. Department of Energy's Office of Science. D.A.P. and D.F.M. are CONICET fellows. M.M. and D.H.M. are members of CIC−CONICET.

Supporting Information Available: This material is available free of charge via the Internet at http://pubs.acs.org.

JA910707R

(42) Lange, C.; Hunte, C. *Proc. Natl. Acad. Sci. U.S.A.* **2002**, *99*, 2800.
(43) Roberts, V. A.; Pique, M. E. *J. Biol. Chem.* **1999**, *274*, 38051.
(44) Cheung, E.; Taylor, K.; Kornblatt, J. A.; English, A. M.; McLendon, G.; Miller, J. R. *Proc. Natl. Acad. Sci. U.S.A.* **1986**, *83*, 1330.
(45) Michel, B.; Bosshard, H. R. *Biochemistry* **1989**, *28*, 244.
(46) Michel, B.; Mauk, A. G.; Bosshard, H. R. *FEBS Lett.* **1989**, *243*, 149.
(47) Michel, B.; Proudfoot, A. E. I.; Wallace, C. J. A.; Bosshard, H. R. *Biochemistry* **1989**, *28*, 456.
(48) Brunori, M.; Sarti, P.; Colosimo, A.; Antonini, G.; Malatesta, F.; Jones, M. G.; Wilson, M. T. *EMBO J.* **1985**, *4*, 2365.
(49) Capitanio, N.; Capitanio, G.; Demarinis, D. A.; De Nitto, E.; Massari, S.; Papa, S. *Biochemistry* **1996**, *35*, 10800.
(50) Hazzard, J. T.; McLendon, G.; Cusanovich, M. A.; Tollin, G. *Biochim. Biophys. Res. Comm.* **1988**, *151*, 429.
(51) Heacock, D. H. *J. Biol. Chem.* **1993**, *268*, 27171.
(52) Schlarb-Ridley, B. G.; Bendall, D. S.; Howe, C. J. *Biochemistry* **2003**, *42*, 4057.
(53) Hunte, C.; Solmaz, S.; Lange, C. *BBA-Bioenergetics* **2002**, *1555*, 21.
(54) Sadeghi, S. J.; Valetti, F.; Cunha, C. A.; Rompo, M. J.; Soares, C. M.; Gilardi, G. *J. Biol. Inorg. Chem.* **2000**, *5*, 730.